Nanoscale Advances

ROYAL SOCIETY OF CHEMISTRY

PAPER

View Article Online
View Journal | View Issue

Cite this: *Nanoscale Adv.*, 2025, **7**, 1872

An octahedral metal oxide nanoparticle-based dual-signal sensing platform for simultaneous detection of histidine and lysine in human blood plasma and urine

Robina Akhtar,[a] Asim Yaqub,*[b] Zia Ul Haq Khan,[c] Ali Turab Jafry [d] and Huma Ajab *[e]

Histidine and lysine serve as essential amino acids in physiological processes and biomarkers for specific diseases, requiring precise detection methods in a variety of samples. This study presents an affordable single colorimetric probe that employs nickel oxide nanoparticles (NiONPs) as an artificial enzyme to detect histidine and lysine, improving conventional analytical limitations. The characterization of NiONPs was executed using SEM-EDX, FE-SEM, FTIR and XRD. The NiONPs demonstrated peroxidase-like catalytic activity on the conversion of TMB to oxidized TMB (oxTMB) in the presence of H_2O_2, utilizing optimization parameters like pH value (3), TMB concentration (10 mM), H_2O_2 concentration (60 mM), and incubation time (18 min). The study revealed that Ni and O atoms are present on the surface of NiONPs, allowing for specific interactions with essential amino acids and temporarily hindering the catalytic activity of oxidized TMB. The method exhibited a low limit of detection (LOD) of 0.07 μM (10–100 μM) for histidine and 1.1 μM (15–150 μM) for lysine with good stability. The proposed strategy was validated with urine and plasma samples, yielding favorable recoveries of 93.6–98.2% in urine and 90.5–96.0% in plasma for histidine and 91.2–94.8% in urine and 88.4–93.3% in plasma for lysine, supporting its selectivity, feasibility, and reliability for practical applications. In the future, this methodology will facilitate the integration of histidine and lysine detection into microfluidic systems using NiONPs as a colorimetric probe.

Received 11th November 2024
Accepted 15th January 2025

DOI: 10.1039/d4na00932k

rsc.li/nanoscale-advances

1. Introduction

Sensor arrays are crucial in chemical and biological analysis for detecting multiple analytes in a single measurement run. Future practical applications require developing single sensor probes with different responses for biologically significant analytes due to their significant roles in chemical/biological processes.[1–3]

Essential amino acids are vital for life activities and human health, and serve as a significant indicator of the health status of living organisms.[4] Histidine, an essential amino acid with an imidazole group, is crucial for human proteins, cell growth, and neurotransmitter roles in both animals and humans,[5–7] and lysine is a basic and charged aliphatic amino acid. It is essential for biochemical synthesis of polyamine, plays a role in the Krebs–Henseleit cycle and is obtained through the diet.[8] Therefore, the selective recognition of histidine and lysine has significant positive implications in biochemistry, medicine, and nutrition.[6]

On the other hand, an abnormal level of histidine and lysine can indicate various diseases like slow growth, liver damage, metabolic disturbance, cancer, Alzheimer's disease, muscle and fat loss *etc.*[9,10] Efficient quantitative determination of histidine and lysine is essential, with techniques such as capillary electrophoresis, chromatography, and electrochemical methods widely reported for detecting these essential amino acids.[11,12] S. Moore and W. H. Stein used ion exchange chromatography in 1948 to analyze amino acids in plasma, urine, and tissue homogenates, earning the Nobel Prize in 1972.[13] Despite its historical significance, this technique presents drawbacks such as lengthy chromatographic separations (60 to 150 minutes) and high costs[14] ($120/sample).

These techniques require professional technicians, and need sample purification, so it is challenging to satisfy the

[a]*Department of Chemistry, COMSATS University Islamabad, Abbottabad Campus, Pakistan. E-mail: robinaakhtarchem@gmail.com*

[b]*Department of Environmental Sciences, COMSATS University Islamabad, Abbottabad Campus, Pakistan. E-mail: asimyaqub@cuiatd.edu.pk*

[c]*Department of Chemistry, COMSATS University Islamabad, Islamabad Campus, Park Road, Islamabad 45550, Pakistan*

[d]*Faculty of Mechanical Engineering, GIK Institute of Engineering Sciences & Technology, Topi, District Swabi, KPK, 23640, Pakistan. E-mail: ali.turab@giki.edu.pk*

[e]*Department of Chemistry, COMSATS University Islamabad, Abbottabad Campus, 22060 Abbottabad, Pakistan. E-mail: humaajab@cuiatd.edu.pk*

requirements for quick identification and on-site analysis of essential amino acids.[7,15] Consequently, there is a need for the development of simple methods that enable untrained users to easily detect analytes and interpret results in resource-limited settings.[16]

Optical sensing techniques like colorimetry, UV-vis spectroscopy, and optical paper-based methods present benefits like low cost, sensitivity, and accelerated detection for identifying essential amino acids, but still encounter obstacles even though they demonstrate a good response.[17–19]

In the field of optical sensing platforms, 2,2-azino-bis (3-ethylbenzothiazoline-6-sulfonic acid) (ABTS) and 3,3′,5,5′-tetramethylbenzidine (TMB) are colorimetric probes due to their high sensitivity, ease of use, and minimal interference. Despite the advantages of natural enzymes, their application is limited due to instability, high cost, and storage issues. Artificial enzymes, often referred to as synthetic enzymes or enzyme mimics, are designed to replicate the catalytic activities of natural enzymes. These structures strive to combine the efficiency and specificity of biological enzymes with the durability and adaptability of synthetic materials, offering flexible catalytic systems suitable for diverse applications and conditions, as well as cost-effective, reproducible alternatives without compromising efficiency and applications.[19–21]

Several studies reported histidine and lysine detection using various nanomaterials and analytical techniques. For instance, Gu *et al.* devised a highly sensitive approach employing CuNCs for detecting histidine, utilizing four molecular triggers: histidine, cysteine, nickel ions, and *N*-ethylmaleimide.[22] Although it is a sensitive method for detection it is a challenging task to produce CuNCs with well-defined and controllable shapes, under ambient conditions. Sudewi *et al.* developed a sensor based on fluorescent iron oxide quantum dots for lysine detection.[23] But, the synthesis process for iron oxide quantum dots involves harsh conditions. Baltzis *et al.* designed a fluorometric assay for histidine using a 96-well plate platform.[24] However, it required meticulous and controlled procedures for histidine analysis. Wei *et al.* designed fluorescent probe DSSH for the detection of histidine.[7] Lavanya *et al.* designed curcumin-based fluorescence sensor DPT [(2*Z*,4*E*,6*E*)-7-(4-(dimethylamino)phenyl)-3-hydroxy-1-phenylhepta-2,4,6-trien-1-one] for lysine detection.[25] Nevertheless, the utilization of an organic framework addressed challenges in detecting both histidine and lysine.

However, there remains a strong demand for a sensitive single colorimetric probe to identify multiple essential amino acids. UV-visible spectroscopy and paper-based detection are valuable for identifying essential amino acids, offering versatility, cost-effectiveness, portability, and quantitative measurements.

In this study, NiONPs have been selected for the first time as a single colorimetric probe for histidine and lysine based on their excellent performance owing to their remarkable redox properties.[26] Their applications span across catalysts and semiconductor sensors owing to their economical nature and commendable catalytic traits.[27] Their high porosity, surface-to-volume ratio, and unique morphology make them effective optical sensors for essential amino acids. The unique catalytic behavior of the Ni(II)/Ni(III) facilitates redox reaction by the absorption of various oxygen anions on the surface which enables NiONPs to function as proficient electron messengers. Sensitivity analyses indicate that NiONPs, especially those featuring abundant nickel vacancies, demonstrate heightened responsiveness towards essential amino acids under standard room temperature conditions.[28–31]

The NiONPs were synthesized using the chemical precipitation method having significant advantages over other methods, including a small and precise particle size distribution, high purity, excellent homogeneity, and reduced reliance on organic solvents.[32] These NiONPs were subjected to characterization through various techniques, including FTIR, SEM-EDX, FE-SEM, and XRD, to assess their suitability for colorimetric detection of essential amino acids. The optimization of various essential parameters was carried out. The sensitivity, selectivity and stability analyses were also performed along with validation studies in real complex samples (blood plasma and urine). Both UV-spectrophotometry and filter paper based platforms were explored and the possible mechanisms were explained.

The sensor leveraged the peroxidase (POD)-like activity of NiONPs, functioning as a nanozyme to catalyze redox reactions. This activity is comparable to that of natural peroxidases, which facilitate the breakdown of hydrogen peroxide and other substrates, and thereby initiate the oxidation of the chromogenic substrate TMB. The notable surface area and accessibility of pores on the NiONPs enabled effective adsorption of both the essential amino acid and TMB onto the nanoparticle surface. Subsequently, the introduction of the essential amino acid inhibited the TMB reaction (as shown in Fig. 5(b)). The developed system generated a colorimetric signal that exhibited a decrease in absorbance and intensity (turn-off) correlating with the concentration of essential amino acids within a significant range.[33] Furthermore, the sensor accurately quantifies essential amino acid trace concentrations in physiological samples, flagging the way for practical on-site detection systems to enhance early diagnostic capabilities. This concept in the future will further help in the integration of histidine and lysine based on a microfluidic system with NiONPs as a colorimetric probe. This integrated platform presents significant potential across various applications, including healthcare, food safety analysis, and point-of-care testing.

2. Experimental procedures

2.1 Materials

All chemicals were used in their analytical grade state without any additional purification. Nickel(II) nitrate hexahydrate [$Ni(NO_3)_2 \cdot 6H_2O$] (97%), histidine (≥98.0%), and sodium hydroxide [NaOH] (97%) were obtained from DAEJUNG chemical reagent company. Gelatin (99.95%), maltose (≥99%), salicylic acid (99%), hydrogen peroxide (30.1%), sodium alginate (≥99%), lysine (≥98%), ascorbic acid (98%), uric acid (99%), and albumin (≥98%) were obtained from Sigma-Aldrich, while creatinine (98%), cysteine (97%), and thiourea (99%) were purchased from MERCK. Double-distilled water and deionized water were consistently employed throughout the experiment.

The gel preparation and dissolution processes involved the utilization of a magnetic stirrer with the model number MSWHP, featuring a revolution speed ranging from 60 to 160 rpm. For the substrate material, round-shaped filter paper was employed and cut using a hole-puncher machine, resulting in a diameter of approximately 0.5 mm.

2.2 Instrumentation

UV/visible spectrometry was performed using a T80 + UV/VIS spectrometer from PG Instruments Ltd (quartz cuvettes with a 1 cm path length served as sample cells). SEM images were captured using a focused ion beam scanning electron microscope (JSM5910, JEOL, Japan) equipped with EDX at a primary voltage of 30 kV. XRD patterns of the synthesized NiONPs were recorded on a JDX 3532 instrument (JEOL, Japan) with graphite-monochromatized Cu Kα radiation within the 10–80° 2θ range. IR spectra ranging from 400 to 4000 cm^{-1} were obtained using an Alpha Centauri FT-IR spectrophotometer.

2.3 Statistical analysis

Optimization/calibration studies and error bars were incorporated into the graphs (to assess the significance of the data) using Origin-Pro (Version 2022, OriginLab). Structural equations were derived through the utilization of ChemDraw Professional (Version 16, 2016), and X'pert High Score Plus (Version 3.0, PANalytical) was employed for processing XRD data and End Note X8.0.2 was utilizing for article citation. Particle size calculations from FE-SEM images were conducted using Image J by calculating the averages. Additionally, the optimization study was performed using ANOVA analysis.

2.4 Chemical precipitation method

In this process, a 0.1 M solution of $Ni(NO_3)_2 \cdot 6H_2O$ was stirred in 100 mL of distilled water at room temperature. Subsequently, a 0.8 M solution of NaOH was added gradually. The obtained mixture was stirred continuously for 4 h while being heated to 80 °C. Following the formation of green-colored precipitates, the excess byproducts were rinsed off with distilled water. The resulting precipitates were then dried for two hours at 80 °C (shown in Fig. 5(a)). Subsequently, the precursor was crushed into a powder and subjected to a temperature of 600 °C for a time of 5 h, resulting in the production of NiONPs with an octahedral structure.[34] The reactions occurring during the synthesis are given below:[32]

$$2NaOH\ (s) \rightarrow 2Na^{+}\ (aq) + 2OH^{-} \quad (1)$$

$$Ni(NO_3)_2 \cdot 6H_2O\ (s) \rightarrow Ni^{2+}\ (aq) + 2NO_3^{-}\ (aq) + 6H_2O\ (aq) \quad (2)$$

$$Ni^{2+}\ (aq) + 2OH^{-} + xH_2O\ (aq) \rightarrow Ni(OH)_2 \cdot xH_2O\ (s)\downarrow \quad (3)$$

$$Ni(OH)_2 \cdot xH_2O\ (s) \xrightarrow{70\ ^\circ C} Ni(OH)_2\ (s) + xH_2O\ (g)\uparrow \quad (4)$$

$$Ni(OH)_2\ (s) \xrightarrow{600\ ^\circ C} NiO\ (S) + H_2O\ (g)\uparrow \quad (5)$$

2.5 Investigation of the peroxidase-like activity of NiONPs (POD)

The proposed peroxidase mimetic based on NiONPs demonstrates the capability to catalyze the oxidation of the chromogenic molecule TMB when exposed to H_2O_2, producing, as a result, a blue-colored solution. To assess its POD-like activity, a 1.5 mg catalyst was introduced into a solution comprising 15 μL of 10 mM TMB and 60 mM H_2O_2 in a 2.5 mL PBS buffer (pH 3), followed by an 18 min incubation time at room temperature. The oxidation of TMB was evaluated through visual observation, detecting the emergence of a blue color, and quantitatively assessed using UV-vis spectroscopy at a specific wavelength of 650 nm. To identify the optimal conditions for the peroxidase-like mimetic oxidation process, experiments were conducted at varying pH levels, TMB and H_2O_2 concentrations, and incubation times.

2.6 Colorimetric detection of histidine and lysine

Aqueous solutions of histidine and lysine at various concentrations were freshly prepared and directly introduced into a 2.5 mL PBS buffer with a pH of 3. Subsequently, NiONPs, along with a fixed amount of 15 μL of 10 mM TMB and 60 mM H_2O_2, were added to the solution. After an 18 minutes incubation period, the absorbance of the obtained solution was measured at 650 nm with a UV-vis spectrophotometer. The concentrations of histidine and lysine were determined by comparing the absorbance difference between the test and control groups against a calibration curve.

To evaluate the anti-interference and selectivity of the developed colorimetric platform, the reactivity of NiONPs towards potential interferents, including gelatin, albumin, creatinine, maltose, salicylic acid, ascorbic acid, uric acid, cysteine, and thiourea, was examined at a consistent concentration of 200 μM.

2.7 Real sample detection

The practical applicability of the synthesized NiONPs was assessed using human blood plasma and urine samples. Urine and blood samples were obtained from human volunteers and informed consents were obtained from human participants of this study. Blood samples were subjected to centrifugation to isolate plasma, which was then stored at 4 °C. Subsequently, both plasma and urine samples were suitably diluted with deionized water. Percentage recoveries were generated by introducing standard histidine and lysine solutions with concentrations ranging from 60 to 100 μM and 100 to 150 μM in these samples. The histidine and lysine concentrations in the real samples were examined by correlating the changes in absorbance intensity at a wavelength of 650 nm with the calibration curve.

2.8 Detection of histidine and lysine using NiONPs on a paper based platform

After the successful detection of histidine and lysine by NiONPs in real samples, we also created a NiONP paper-based platform

for the rapid detection of histidine and lysine, leveraging its high detection capability for these essential amino acids. In this experiment, circular sections of filter paper with a diameter of 0.5 mm were cut. Each section was then coated with a layer of sodium alginate gel, prepared by dissolving 300 mg of sodium alginate in 6 mL of distilled water and incorporating 1.5 mg of NiONPs. This coating was applied to hold aqueous samples on the paper. The paper was then coated with freshly prepared H_2O_2 and TMB solution. A bluish color appeared on the paper after a few minutes, indicating the formation of the oxidized product of TMB. The reduction in TMB oxidation was caused by the addition of histidine and lysine solutions with varying concentration. The blue color of oxTMB on the filter paper began to fade after 10 minutes with different extents depending on the concentration of the histidine and lysine solution.

3. Results and discussion

3.1 SEM and FE-SEM with EDX characterization

SEM is widely employed for characterizing materials due to its extensive utility. The underlying principle of electron microscopy shares similarities with optical microscopy, but with a crucial distinction: while visible light serves as the incident source in optical microscopy, electron microscopy utilizes accelerated electrons. The electron beam's small wavelength enables the visualization of extremely infinitesimal features in the sample. Signals generated through the interaction of electrons with the sample provide understanding into the chemical composition and the surface morphology (texture) of the material.[35]

The surface morphological characteristics of the produced NiONPs are illustrated in Fig. 1(a and b), demonstrating a porous flaky structure reminiscent of broccoli and some particles show homogeneous spherical shapes[36] with minor aggregation. The tendency to aggregate is a prevalent phenomenon, attributed to robust intraparticle interactions resulting from the high surface energy inherent in nanoparticles.[37] The result signifies that these particles directly contribute to the detection of the essential amino acids by promoting a high surface-to-volume ratio, thereby enhancing the surface to facilitate an accelerated reaction.

The examination and analysis of SEM results were conducted to gain an initial consideration of the internal morphological and structural features of NiONPs. On the other hand, due to factors such as instrument magnification, resolution, and manual adjustments, SEM often provides results at the micron level and may display artificial pores or fractures. Therefore, following SEM observations, FE-SEM was employed to examine specific regions of the NiONPs, aiming for perfect characterization of their internal morphological structures at the nanoscale. The experimental results obtained from FE-SEM are depicted in Fig. 1(c and d).[38] An examination using FE-SEM shows that the NiONPs exhibit an octahedron-like shape consisting of 8 equilateral triangular surfaces and 12 identical edges,[39] devoid of any indications of aggregation, and are polydispersed, through an average particle size of nearly 53.9 nm (Fig. 1(e)), which was determined using automated analysis with image processing software like Image J. The grain diameter was measured by setting the scale, and subsequently, the particle size distribution was plotted in Origin using its specific distribution plotting tools. This shape significantly influences their optical and electronic properties because of its high surface area and excellent conductivity. This shape also revealed that the particles have exceptional durability and hardness.

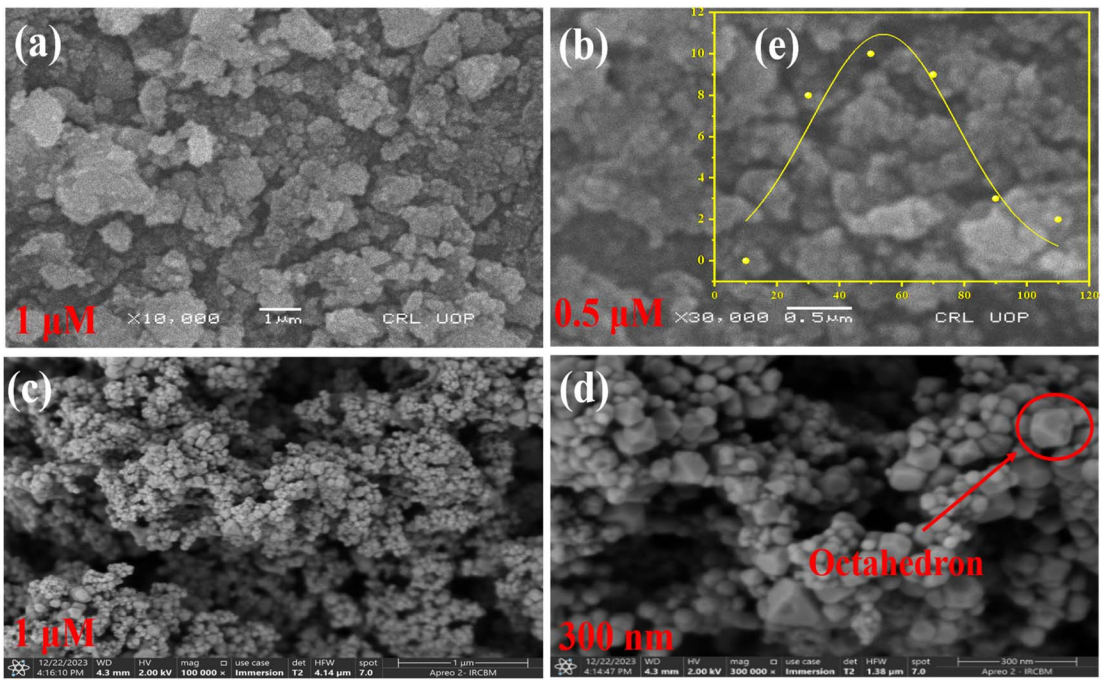

Fig. 1 (a and b) SEM images; (c and d) FE-SEM images of NiO nanoparticles; (e) particle size distribution of NiO nanoparticles.

Microanalysis techniques such as the Energy Dispersive X-ray technique (EDX) are used to identify and analyze the elemental compositional of specimens. The process involves measuring the quantity and energy of X-rays radiated by the specimens when excited by an electron beam, enabling elemental identification. Typically, EDX is utilized in conjunction with electron microscopy techniques such as Scanning Electron Microscopy (SEM) and Transmission Electron Microscopy (TEM).[35,40]

In order to evaluate the elemental compositions of the NiONPs, EDX analysis was performed (Fig. 2(c)). The resulting profiles of the synthesized nanoparticles verified the predominant presence of nickel and oxygen, with no discernible presence of other impurities.

3.2 FT-IR and XRD characterization

Fourier-Transform Infrared spectroscopy (FT-IR) is a spectroscopic method that entails the measurement of sample molecule functional groups through infrared radiation. The resulting IR spectrum is graphically represented with absorbance and transmittance on the vertical axis and frequency or wavelength on the horizontal axis. In the IR spectrum, bands provide crucial information about the nature and strength of bonds, molecular structures, interactions, and the existence of functional groups within the sample.[35,41]

The FT-IR spectrum of NiONPs is illustrated in Fig. 2(a), revealing distinct absorption peaks. Following calcination, the FT-IR spectra of NiONPs display a robust band at 443 cm^{-1} and 663 cm^{-1}, indicating the stretching vibrations of the Ni–O bond. The peak at 1398 cm^{-1} can be ascribed to the bending and stretching vibrations of the –OH group, which is adsorbed on the catalyst surface from the atmosphere during FT-IR analysis.[42] The band at 1014 cm^{-1} is associated with the OH band,[43] and the peak at 1601 cm^{-1} is indicative of H–O–H bonding.[44] Additionally, the prominent band observed at 3430 cm^{-1} is attributed to the symmetrical stretching vibrations of $^{-}$OH groups due to the tendency of the calcined powders to physically absorb water.[45] These findings provide crucial insights into the structure, functional groups, and purity of the NiONPs prepared and show their enhanced optical properties.

X-ray diffraction (XRD) is a commonly used technique for characterizing NPs. It typically provides information about the

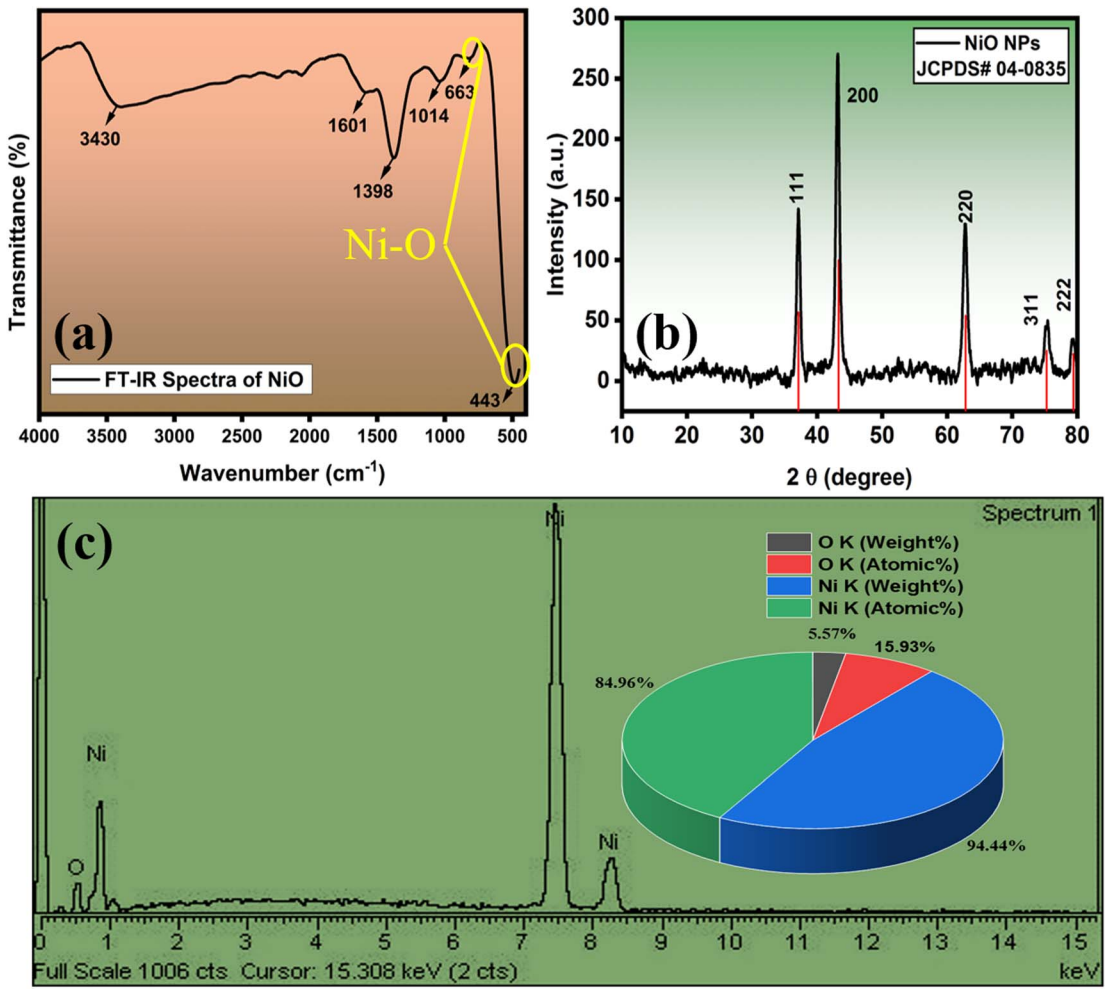

Fig. 2 (a) FT-IR spectrum of NiONPs; (b) XRD pattern of NiONPs; (c) EDX spectrum of NiONPs.

phase composition, crystalline structure, lattice parameters, and crystalline grain size through the Scherrer equation. It relates the broadening of diffraction peaks to the sub-micrometer size of crystallites in the material.[35,41]

The structural analysis of the synthesized NiONPs, as described in Fig. 2(b), revealed diffraction peaks at Bragg's 2θ angles of 37.228°, 43.254°, 62.830°, 75.352°, and 79.341°. These peaks indicate a strong atomic orientation along the crystallographic planes (111), (200), (220), (311), and (222), respectively. The absence of additional peaks in the XRD spectra signifies that the NiONPs exist in a single phase, crystallizing in a cubic structure, which aligns well with JCPDS card no. 04-0835, suggesting high purity of the NiONPs. Utilizing the Debye–Scherrer equation, the crystallographic parameter of crystallite size was determined.[46]

$$D = \frac{K\lambda}{\beta \cos \theta} \quad (6)$$

where Bragg's angle is represented by θ, the shaping factor is given by K, the wavelength of X-rays is denoted by λ, and the full width at half maximum is represented by β. The estimated crystallite size for NiONPs came out to be 13 nm.[47] The relationship between crystallite size and peak intensity was examined, revealing that as the peak width decreases, the size of the crystallites increases. The XRD pattern of NiONPs showed pronounced peak broadening, indicative of the existence of oxygen vacancies[48] and their 13 nm crystallite size indicated high crystallinity. This nanosized and highly crystalline structure is expected to enhance the interaction of the NiONPs with the essential amino acids.

As shown in Fig. 3(a), a blue color appeared upon the catalytic reaction of NiONPs with TMB and H_2O_2 solution, and the addition of histidine and lysine shows fading of color under experimental conditions. These results clearly suggest the obtained NiONPs have exceptional POD-like activity and are highly dependent on the pH, concentration of TMB and H_2O_2, and time. Experiments on long-term stability were conducted to examine the catalytic activity of NiONPs. The solution was kept at room temperature without any particular protection, and periodic measurements of the POD activity were made (Fig. 3(b)). Nineteen days later, no noticeable reduction in the catalytic activity was observed. It has been shown that, under normal conditions, NiONPs may sustain remarkable catalytic activity for a longer duration.

3.3 Optimization of detection conditions

The catalytic activity of NiONPs was investigated by systematically changing one parameter at a time, including pH, concentration of TMB and H_2O_2, and reaction time. During the investigation, absorbance was used as the criterion for optimizing the detection conditions.

The pH impact on the POD catalytic activity of NiONPs was examined by adjusting the pH of the buffer solution within the range of pH 1 to pH 9. The absorbance peak at 650 nm was monitored during this variation. The results depicted in Fig. 4(a) indicate a pH-dependent trend in the catalytic activities of NiONPs. Initially, these activities increased with a rise in pH, reaching their peak at pH 3. However, beyond pH 3, the activity of NiONPs diminishes significantly due to the scarcity of H^+ ions. This reduces the number of protonation processes, which in turn makes the adsorption and interaction of the substrate less efficient. Consequently, pH 3 was selected as the optimal condition for further experiments, as it yielded the highest absorbance due to improved electron transfer activity. At this pH, TMB oxidation is more effective, as it promotes a faster electron transfer process and enhances the overall catalytic process.

A study was carried out to explore the impact of H_2O_2 and TMB concentrations on absorbance, as depicted in Fig. 4(b and c). The findings specified that the maximum absorbance was

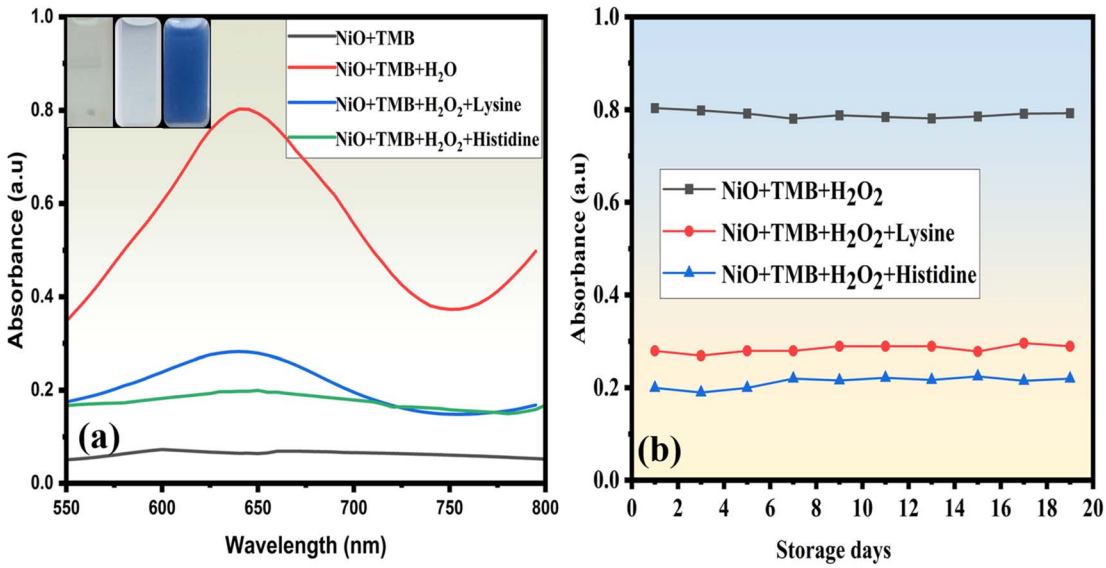

Fig. 3 (a) UV-vis absorption spectra of the NiONPs with and without the addition of histidine and lysine; (b) stability of NiONPs (catalytic activity and POD-like activity).

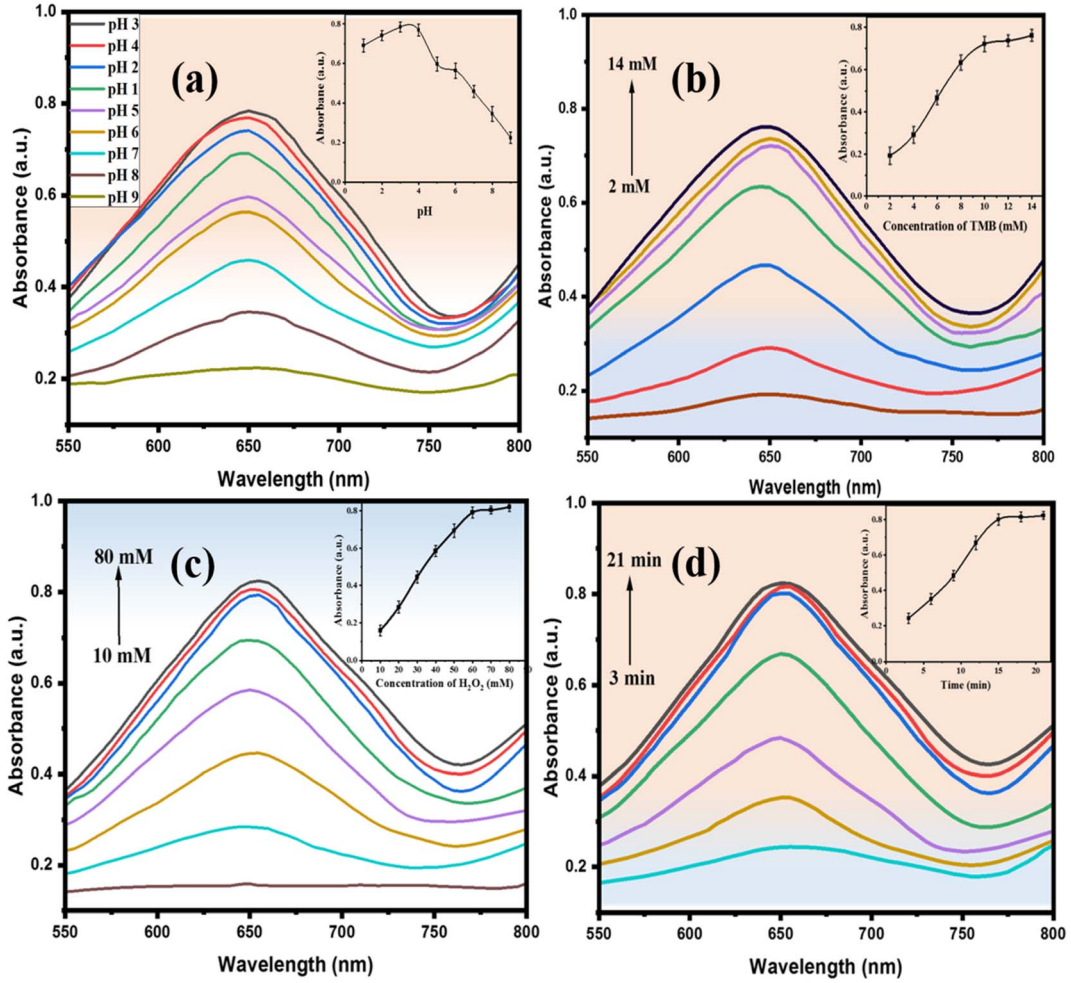

Fig. 4 (a) Effects of pH, (b) effect of TMB, (c) effect of H_2O_2, (d) impact of incubation time on the POD-mimetic activity of NiONPs.

reached when utilizing 60 mM H_2O_2 and 15 μL of 10 mM TMB. While the absorbance of oxidized TMB increased with increasing concentrations of both TMB and H_2O_2, the relative activities also increased accordingly and reached a maximum after 10 mM for TMB and 60 mM for H_2O_2. Consequently, concentrations of 10 mM TMB and 60 mM H_2O_2 (15 μL) were selected for the colorimetric assay because they provided an optimal response. Beyond these concentrations, a linear increase in response was observed due to the fact that, with higher concentrations, equilibrium is reached more rapidly in the reaction, compared to lower concentrations of TMB and H_2O_2.

Similarly, the impact of reaction time on the absorbance and catalytic reactivity of NiONPs was explored. Fig. 4(d) illustrates the absorption studies conducted over time, at room temperature, in a buffer solution with a pH of 3. The catalytic activity of NiONPs exhibited a positive correlation with the contact time, reaching equilibrium within 18 minutes. Under identical conditions, NiONPs achieved their highest catalytic activity in 18 min.

Considering all of the above parameters, the optimum conditions for the present colorimetric sensing of histidine and lysine are: pH = 3; TMB = 15 μL of 10 mM; H_2O_2 = 60 mM; and time = 18 min.

3.4 Statistical analysis

One way ANOVA was applied to determine the effect of each variable pH, TMB concentration, H_2O_2 concentration, and time with absorbance data. ANOVA results showed that data were significantly different from each other (Table 1).

3.5 Catalytic mechanism

A colorimetric assay was performed using a catalytic reaction to oxidize TMB. Here, 15 μL of 10 mM TMB was added into the solution containing 1.5 mg NiONPs, 2.5 mL PBS solution (pH 3), and 60 mM H_2O_2. TMB was utilized to initiate the reaction, after which the reaction's color was noted and UV-vis spectra were obtained.[49]

Most catalytic mechanisms of POD mimics can be classified into two types: one involves the generation of intermediates, such as superoxide radicals and hydroxyl radicals, during the catalytic process, and the other is based on the electron transfer mechanism.[50]

Based on the preceding examination, it can be inferred that the POD exhibited by the NiONPs could be attributed to the following factors. Primarily, the NiONPs present a distinct optical property, which is able to break down the O–O bond in

Table 1 One way ANOVA for various optimized parameters

Variables	Source of variation	SS	df	MS	F	*P*-value	F_{crit}
pH	Between groups	88.11	1	88.11149	23.37	0.00018	4.49
	Within groups	60.31	16	3.769 536			
	Total	148.42	17				
TMB	Between groups	194.62	1	194.6169	20.79	0.00065	4.74
	Within groups	112.32	12	9.359 744			
	Total	306.93	13				
H_2O_2	Between groups	7895.013	1	7895.013	26.31	0.00015	4.60
	Within groups	4200.449	14	300.0321			
	Total	12 095.46	15				
Time	Between groups	454.99	1	454.99	21.63	0.00056	4.74
	Within groups	252.34	12	21.028			
	Total	707.34	13				

H_2O_2 into a highly oxidizing OH˙ radical.[51] The Ni^{2+} within the center of NiO may play a vital role by activating the H_2O_2 molecules to form highly reactive hydroxyl species (OH˙).

Second, the generated OH˙ radicals exhibit strong oxidizing power, enabling them to oxidize a POD substrate like TMB in the presence of H_2O_2, producing a blue color as shown in Fig. 3(a). Without hydrogen peroxide, the formation of oxidized TMB is not possible. Consequently, both OH˙ radical generation and electron transfer properties contribute to the material's exceptional POD-like activity.[52,53] Predictably, a higher amount of NiONPs would give rise to more OH˙ radicals and stronger peak intensity.[54] This is due to the enhanced surface area providing more active sites for the catalytic reaction, potentially leading to higher catalytic efficiency.

The reaction for the formation of oxidized TMB is given below:

$$2H_2O_2 + TMB \xrightarrow{NiO\ NPS} \text{oxidized TMB (blue color)} + 2H_2O + O_2 \quad (7)$$

Different concentrations of histidine and lysine were examined for catalytic measurements, and absorbance changes were monitored in spectrum mode after 10 minutes of the catalytic reaction. The absorbance of the resulting solution was measured at 650 nm, which corresponds to the fading of the solution.[55] As the concentrations of histidine and lysine increased, the absorbance intensities decreased. Acting as reducing agents, these essential amino acids contain specific functional groups (an imidazole in histidine and an extra amino group in lysine), which can bind to NiO NPs or interact with the generated OH˙ radicals. This interaction influences the NiO-catalyzed oxidation by modifying electron transfer efficiency or radical production. The

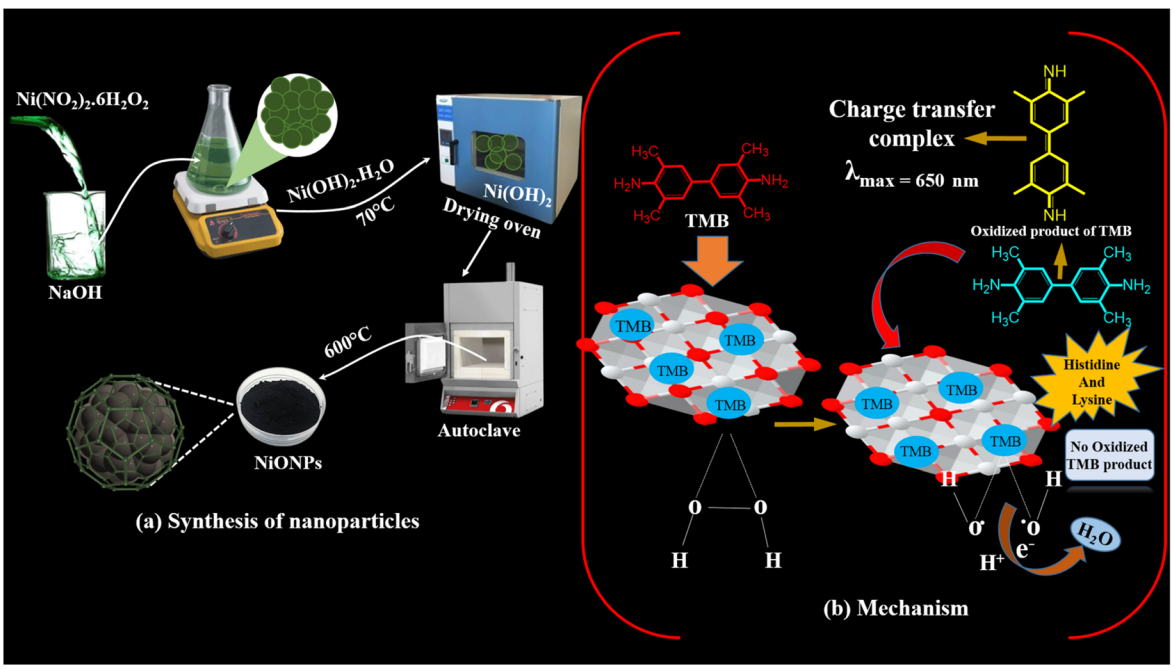

Fig. 5 (a) Synthesis of NiONPs through the chemical precipitation method; (b) mechanism of peroxidase mimic activity of NiONPs in the absence and presence of histidine and lysine.

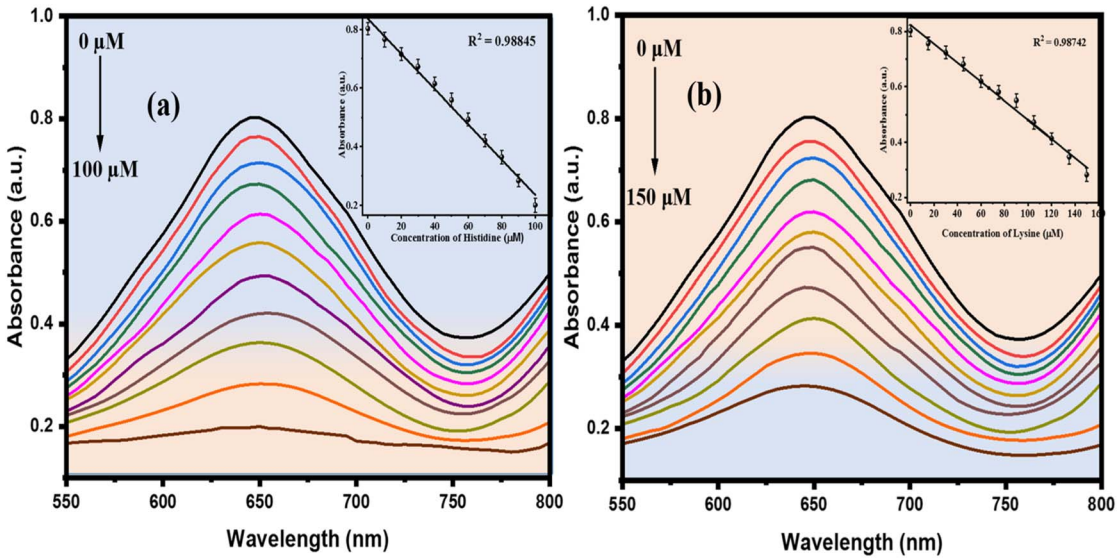

Fig. 6 (a) UV-vis absorption spectra of the proposed colorimetric sensing platform recorded for various histidine concentrations, demonstrating the calibration response. (b) UV-vis absorption spectra of the proposed colorimetric sensing platform recorded for various lysine concentrations, demonstrating the calibration response.

absorbance intensities showed a linear decrease within the ranges of 10–100 μM and 15–150 μM and after this, no noticeable changes in absorption intensities were observed (Fig. 6(a and b)). The relationship between A (650 nm) and the concentration of histidine showed a linear fit with $R^2 = 0.98778$, while lysine had $R^2 = 0.9851$. The LOD was determined using 3 times the standard deviation (3σ) and the slope (S) of the linear equation for histidine and lysine, resulting in values as low as 0.07 μM (70 nM) for histidine and 1.1 μM (1100 nM) for lysine.

Table 2 shows the linearity and LOD of the colorimetric method used for the histidine and lysine. In comparison, our method demonstrated a lower LOD and a good linear range.

3.6 Selectivity of histidine and lysine determination

Several molecules, *i.e.* gelatin, albumin, maltose, salicylic acid, creatinine, ascorbic acid, uric acid, cysteine, and thiourea, were used in the experiment to examine the selectivity of the sensor. The concentrations of these molecules were 200 μM whereas those of histidine and lysine were 100 μM and 150 μM which are one or two times lower than the concentration of interfering molecules. The POD-like activity of NiONPs was unaffected by the presence of interfering molecules (as shown on Fig. 7). There was a slight interaction with cysteine, but it was less noticeable compared to that with histidine and lysine. The strong interaction of NiONPs with histidine and lysine may inhibit the peroxidase-like activity, observed by measuring the extinction spectra of NiONPs with and without these substances.

The surface of NiONPs facilitates the formation of binding sites that increase the affinity for histidine and lysine. Additionally, the size, shape, and structure of histidine and lysine molecules enable them to more effectively fit into the active sites of the NiONPs. The complex and bulky structures of other analytes may hinder their interaction with NiONPs. The findings suggest that NiONPs exhibit good selectivity for histidine and lysine.

Table 2 Comparison of the detection limits for histidine and lysine of different NP-based sensors with that in the present study

No.	Material	Analyte	Limit of detection	Linear range	Reference
1	Nitrogen-doped carbon nanoparticle	Histidine	150 nM	0.5–60 μM	56
2	Imidazole-functionalized silicon quantum dots	Histidine	0.52 μM	1.6–200 μM	57
3	TAMSMB-Ni^{2+}	Histidine	0.49 μM	—	58
4	HPTS	Lysine	3.106 μM	—	59
5	Copper nanoclusters	Lysine	5.5 μM	10.0 μM–1.0 mM	60
6	GQD/AuNPs	Lysine	16.14 μM	—	61
7	L-Cysteine modified carbon quantum dots	Lysine	0.30 mM	—	62
8	MAFC	Lysine	100 μM	—	8
9	NiO	Histidine	0.07 μM	10–100 μM	Present work
		Lysine	1.1 μM	15–150 μM	

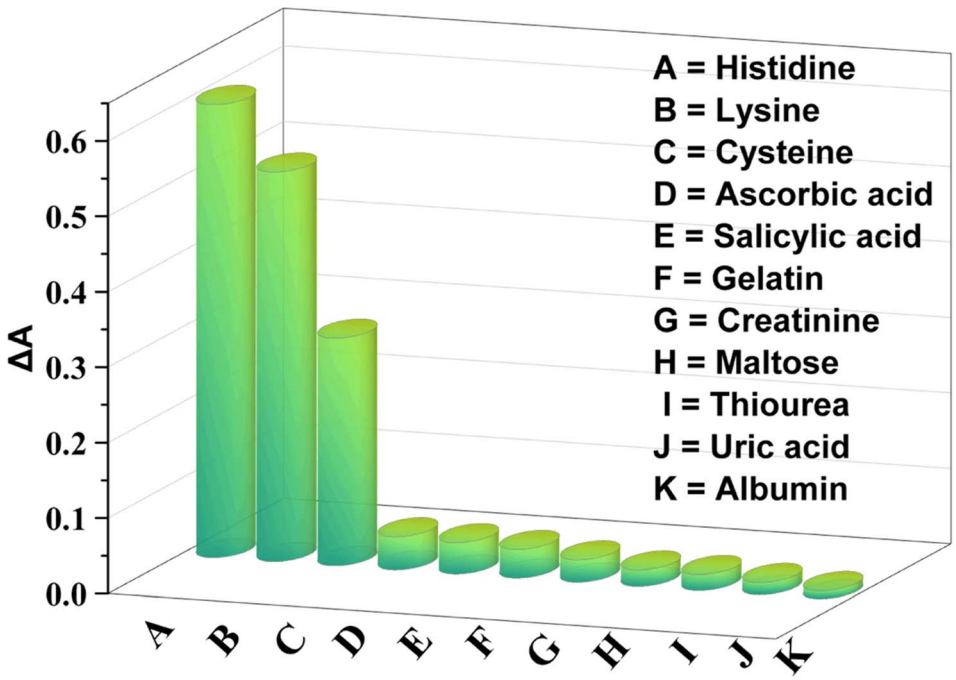

Fig. 7 Selectivity of NiONPs for histidine and lysine.

3.7 Determination of histidine and lysine in plasma and urine samples

The possibility of applying the sensor for detecting histidine and lysine in practical samples was examined using plasma and urine obtained from a healthy person. The samples showed no detectable results when tested without spiking. Therefore, the samples were spiked with specific concentrations of histidine and lysine after being diluted with deionized water. The NiONP catalytic activity was marginally inhibited as compared to a control sample of non-spiked urine and plasma. The spiked plasma and urine samples of different concentrations of histidine and lysine, however, exhibited comparative inhibiting properties towards the POD-like activity of NiONPs. The recovery ranges of histidine are from 93.6–98.2% for the urine sample and 90.5–96.0% for plasma and the recovery ranges of lysine are from 91.2–94.8% for urine and 88.4–93.3% for plasma. As demonstrated in Table 3, the results confirm our method's ability to practically detect histidine and lysine in real samples.

Table 3 Determination of histidine and lysine in urine and blood plasma samples using the current developed method

Urine sample

	Histidine added (μM)	Histidine found (μM)	Relative %	Lysine added (μM)	Lysine found (μM)	Relative %
1	60	56.2	93.6	100	91.2	91.2
2	80	76.0	95.0	120	110.0	91.6
3	100	98.2	98.2	150	142.2	94.8

Plasma sample

	Histidine added (μM)	Histidine found (μM)	Relative %	Lysine added (μM)	Lysine found (μM)	Relative %
1	60	54.3	90.5	100	89.8	89.8
2	80	73.1	9 1.3	120	106.1	88.4
3	100	96.0	96.0	150	140.0	93.3

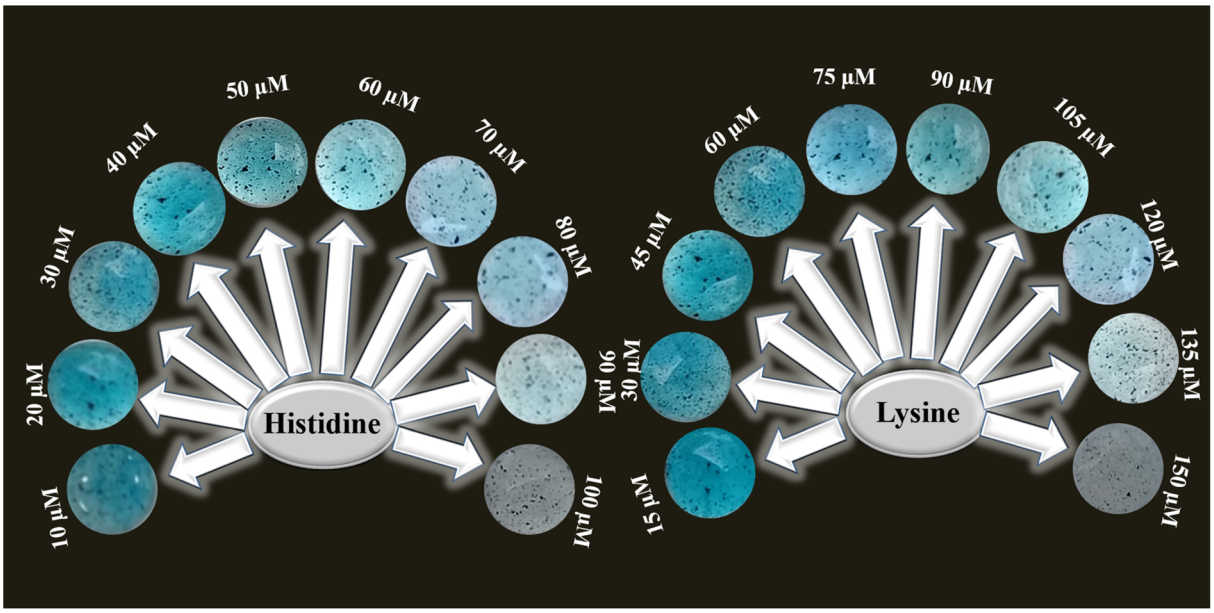

Fig. 8 Paper based assays of the NiONPs after 10 min in the presence of variable concentrations of histidine and lysine from 10–100 µM and 15–150 µM.

3.8 Sensing of histidine and lysine using the NiONP paper based platform

To exploit the practical uses of a NiONP-based colorimetric probe for detecting histidine and lysine, a user-friendly and sensitive paper-based platform was employed. The fixed network of microchannels within cellulose fibers enables the detection of histidine and lysine, utilizing the readily available cost-effective paper substrate. The sodium alginate coating does not alter the physical structure of the paper substrate. Upon adding a mixture of fresh solution of TMB and H_2O_2 to the sodium alginate gel containing NiONPs coated on circular paper, the oxidized form of TMB turned the paper bluish. Introduction of histidine and lysine solution inhibits the oxidation process of TMB. After 10 minutes, the bluish color gradually fades to different extents, corresponding to various concentrations of histidine and lysine solutions, as illustrated in Fig. 8.

4. Conclusions

In this research, simultaneous detection of the essential amino acids histidine and lysine was conducted using a portable and simple colorimetric sensor (UV-vis spectroscopy and paper-based sensor) that has been developed. A NiONP nanoprobe with high sensitivity and inherent POD-like catalytic activity was synthesized by a chemical precipitation process and was characterized by SEM-EDX, FE-SEM, XRD, and FT-IR methods. The system comprised NiONPs, TMB, and H_2O_2 as reacting substances for the essential amino acids, demonstrating satisfactory analytical response. In addition, compared with previously reported methods for the detection of histidine and lysine, the sensor of this study can achieve lower detection limits of 0.07 µM for histidine and 1.1 µM for lysine within the ranges of 10–100 µM and 15–150 µM and had good stability. Moreover, the proposed method's suitability was confirmed by analyzing urine and blood samples containing spiked histidine and lysine.

Data availability

Data will be made available on request.

Conflicts of interest

There are no conflicts to declare.

References

1 K. Länge, Bulk and surface acoustic wave sensor arrays for multi-analyte detection: A review, *Sensors*, 2019, **19**(24), 5382.
2 Y. Chen, *et al.*, An ultrafast BODIPY single molecular sensor for multi-analytes (acid/base/Cu2+/Bi3+) with different sensing mechanism, *Dyes Pigm.*, 2019, **165**, 279–286.
3 M. Oguz, *et al.*, A basket-type fluorescent sensor based calix [4] azacrown ether for multi-analytes: Practicability in living cells and real sample, *Microchem. J.*, 2021, **167**, 106279.
4 A.-F. Yang, *et al.*, Stable Lanthanide–Organic Framework as a Luminescent Probe To Detect Both Histidine and Aspartic Acid in Water, *Inorg. Chem.*, 2019, **58**(9), 6356–6362.
5 J. Moro, *et al.*, Histidine: A systematic review on metabolism and physiological effects in human and different animal species, *Nutrients*, 2020, **12**(5), 1414.
6 K. Wang, *et al.*, Highly pH-Responsive Sensor Based on a EuIII Metal–Organic Framework with Efficient Recognition of Arginine and Lysine in Living Cells, *Anal. Chem.*, 2023, **95**(11), 4992–4999.
7 P. Wei, *et al.*, A novel fluorescent probe based on a tripeptide-Cu (II) complex system for detection of histidine and its

application on test strips and smartphone, *Spectrochim. Acta, Part A*, 2023, **290**, 122290.
8 L. Zeußel, *et al.*, Colorimetric Method for Instant Detection of Lysine and Arginine Using Novel Meldrum's Acid-Furfural Conjugate, *ChemistrySelect*, 2021, **6**(27), 6834–6840.
9 Y. Zhou and J. Yoon, Recent progress in fluorescent and colorimetric chemosensors for detection of amino acids, *Chem. Soc. Rev.*, 2012, **41**(1), 52–67.
10 Y. Jiao, *et al.*, Colorimetric detection of L-histidine based on the target-triggered self-cleavage of swing-structured DNA duplex-induced aggregation of gold nanoparticles, *Microchim. Acta*, 2018, **185**, 1–6.
11 X. Chen, *et al.*, Highly sensitive and selective colorimetric sensing of histidine by NAC functionalized AuNPs in aqueous medium with real sample application, *Microchem. J.*, 2021, **160**, 105661.
12 M. Farooq, *et al.*, Tuning the structure and properties of MoS2-SrTiO3 nanocomposite and its enzyme mimic behavior for enhanced optical sensing and measurement of H2O2 in biological samples, *Measurement*, 2023, **216**, 112901.
13 G. Gałęzowska, J. Ratajczyk and L. Wolska, Determination of amino acids in human biological fluids by high-performance liquid chromatography: Critical review, *Amino Acids*, 2021, **53**(7), 993–1009.
14 D. W. Johnson, Free amino acid quantification by LC–MS/MS using derivatization generated isotope-labelled standards, *J. Chromatogr. B*, 2011, **879**(17–18), 1345–1352.
15 I. Ullah, *et al.*, Sensitive and cost-effective colorimetric sensor based on enzyme mimic MoS2@ CoTiO3 nanocomposite for detection of hydrogen peroxide in milk and tap water, *J. Food Compos. Anal.*, 2023, **124**, 105689.
16 M. Buzdar, *et al.*, Paper based colorimetric sensor using novel green magnetized nanocomposite of pinus for hydrogen peroxide detection in water and milk, *Food Biosci.*, 2023, **55**, 103014.
17 L. Wang, *et al.*, Constructing difunctional histidine-modified magnetic hybrid nanozymes as capture probes and signal amplifiers for the sensitive colorimetric detection of Salmonella Typhimurium in food, *Microchem. J.*, 2022, **182**, 107917.
18 A. P. VS, *et al.*, Colorimetric sensors for rapid detection of various analytes, *Mater. Sci. Eng. C*, 2017, **78**, 1231–1245.
19 A. Khan, *et al.*, An experimental and theoretical aided 2D MoS2 nanoflowers strategy for rapid visual sensing of Gallic acid in food and clinical matrixes, *Appl. Surf. Sci. Adv.*, 2024, **20**, 100581.
20 P. K. Boruah, *et al.*, Porous Nitrogen-Doped Crumpled Graphene Nanoparticles: A Metal-Free Nanozyme for Selective Detection of Dopamine in Aqueous Medium and Human Serum, *ACS Appl. Nano Mater.*, 2023, **6**(3), 1667–1677.
21 L. Zheng, *et al.*, Artificial enzyme innovations in electrochemical devices: advancing wearable and portable sensing technologies, *Nanoscale*, 2024, **16**(1), 44–60.
22 Z. Gu and Z. Cao, Molecular switch-modulated fluorescent copper nanoclusters for selective and sensitive detection of histidine and cysteine, *Anal. Bioanal. Chem.*, 2018, **410**, 4991–4999.
23 S. Sudewi, *et al.*, Enhanced fluorescent iron oxide quantum dots for rapid and interference free recognizing lysine in dairy products, *Spectrochim. Acta, Part A*, 2022, **279**, 121453.
24 D. Baltzis, *et al.*, Smartphone-Based High-Throughput Fluorimetric Assay for Histidine Quantification in Human Urine Using 96-Well Plates, *Molecules*, 2023, **28**(17), 6205.
25 R. Lavanya, *et al.*, Selective fluorescence turn-off detection of lysine by a curcumin derivative with real sample analysis, *J. Photochem. Photobiol., A*, 2023, **444**, 115008.
26 M. Li, *et al.*, Coaxial electrospinning synthesis of size-tunable CuO/NiO hollow heterostructured nanofibers: Towards detection of glucose level in human serum, *Colloids Surf., B*, 2023, **222**, 113047.
27 H. Zhu, *et al.*, Electronic structure analysis of NiO quantum dot-modified jackfruit-shaped ZnO sensors and sensing properties investigation of their highly sensitive and selective for butyl acetate, *J. Colloid Interface Sci.*, 2023, 466–479.
28 N. Raeisi-Kheirabadi and A. Nezamzadeh-Ejhieh, The Experimental Design Approach in Square-Wave Voltammetric Determination of Tamoxifen by NiO-CPE, *ChemistrySelect*, 2022, **7**(44), e202203788.
29 Y.-F. Sun, *et al.*, Highly sensitive electrochemical detection of Pb (II) based on excellent adsorption and surface Ni (II)/Ni (III) cycle of porous flower-like NiO/rGO nanocomposite, *Sens. Actuators, B*, 2019, **292**, 136–147.
30 Q. Liu, *et al.*, NiO nanoparticles modified with 5, 10, 15, 20-tetrakis (4-carboxyl pheyl)-porphyrin: promising peroxidase mimetics for H2O2 and glucose detection, *Biosens. Bioelectron.*, 2015, **64**, 147–153.
31 M. Ghadiri, M. Ghashghaee and M. Ghambarian, Influence of NiO decoration on adsorption capabilities of black phosphorus monolayer toward nitrogen dioxide: periodic DFT calculations, *Mol. Simul.*, 2020, **46**(14), 1062–1072.
32 S. S. Narender, *et al.*, Nickel oxide nanoparticles: a brief review of their synthesis, characterization, and applications, *Chem. Eng. Technol.*, 2022, **45**(3), 397–409.
33 R. Akhtar, *et al.*, Overcoming challenges and enhancing Precision: Advancements in optical Bio (sensors) and wearable devices for essential amino acid detection integrated with nanotechnology, *Opt Laser. Technol.*, 2024, **177**, 111193.
34 M. Bonomo, Synthesis and characterization of NiO nanostructures: a review, *J. Nanopart. Res.*, 2018, **20**(8), 222.
35 W. Ahmad, *et al.*, A review on current trends in the green synthesis of nickel oxide nanoparticles, characterizations, and their applications, *Environ. Nanotechnol., Monit. Manage.*, 2022, **18**, 100674.
36 Shehala, *et al.*, Carboxymethyl cellulose-NiO nanoparticles as peroxidase mimic for sensitive colorimetric detection of hydrogen peroxide, *Chem. Pap.*, 2023, **77**(3), 1299–1316.

37 M. W. Alam, *et al.*, Effect of Mo doping in NiO nanoparticles for structural modification and its efficiency for antioxidant, antibacterial applications, *Sci. Rep.*, 2023, **13**(1), 1328.
38 D. Wu, *et al.*, Fine Structure Characterization of Representative Coal-Bearing Rocks of the Late Carboniferous Taiyuan Formation in Huainan Coalfield: Combined SEM, FESEM, and μCT Techniques, *ACS Omega*, 2024, 2850–2865.
39 D. Huang, *et al.*, Template-free synthesis of NiO skeleton crystal octahedron and effect of surface depression on electrochemical performance, *J. Sol-Gel Sci. Technol.*, 2019, **89**, 511–520.
40 M. Scimeca, *et al.*, Energy Dispersive X-ray (EDX) microanalysis: A powerful tool in biomedical research and diagnosis, *Eur. J. Histochem.*, 2018, **62**(1), 2841.
41 S. Mourdikoudis, R. M. Pallares and N. T. Thanh, Characterization techniques for nanoparticles: comparison and complementarity upon studying nanoparticle properties, *Nanoscale*, 2018, **10**(27), 12871–12934.
42 S. D. Khairnar and V. S. Shrivastava, Facile synthesis of nickel oxide nanoparticles for the degradation of Methylene blue and Rhodamine B dye: a comparative study, *J. Taibah Univ. Sci*, 2019, **13**(1), 1108–1118.
43 F. Alharbi, *et al.*, Facile development of Mn doped NiO nanoarrays supported on a reduced graphene oxide nanocomposite as a supercapacitor, *Energy Fuels*, 2023, **37**(16), 12225–12235.
44 P. Vijayadarshan, *et al.*, Large scale synthesis of nickel oxide (NiO) by self propagated combustion reaction, *Mater. Sci. Res. India*, 2017, **14**, 37–42.
45 M. Bhoye, *et al.*, Eco-Friendly Synthesis of Ni/NiO Nanoparticles Using Gymnema sylvestre Leaves Extract for Antifungal Activity, *J. Compos. Sci.*, 2023, **7**(3), 105.
46 S. E. Medeiros, *et al.*, Influence of particle size on the electrocatalytic activity and optical properties of nio nanoparticles, *Mater. Sci. Eng. B*, 2023, **289**, 116266.
47 F. Fazlali, A. reza Mahjoub and R. Abazari, A new route for synthesis of spherical NiO nanoparticles via emulsion nano-reactors with enhanced photocatalytic activity, *Solid State Sci.*, 2015, **48**, 263–269.
48 T. Zahra and K. S. Ahmad, Structural, optical and electrochemical studies of organo-templated wet synthesis of cubic shaped nickel oxide nanoparticles, *Optik*, 2020, **205**, 164241.
49 Y. Chen, *et al.*, CuMnO2 nanoflakes as pH-switchable catalysts with multiple enzyme-like activities for cysteine detection, *Sens. Actuators, B*, 2019, **279**, 374–384.
50 K. Wu, *et al.*, Cobalt tuned copper sulfide on montmorillonite: Peroxidase-like activity, catalytic mechanism and colorimetric sensing of hydrogen peroxide, *Colloids Surf., A*, 2020, **602**, 125063.
51 N. Song, *et al.*, Confinement of prussian blue analogs boxes inside conducting polymer nanotubes enables significantly enhanced catalytic performance for water treatment, *Adv. Funct. Mater.*, 2022, **32**(34), 2204751.
52 Z. Mu, *et al.*, Dual mechanism enhanced peroxidase-like activity of iron–nickel bimetal–organic framework nanozyme and its application for biosensing, *ACS Sustain. Chem. Eng.*, 2022, **10**(9), 2984–2993.
53 Y. Choi, J. H. Hwang and S. Y. Lee, Recent trends in nanomaterials-based colorimetric detection of pathogenic bacteria and viruses, *Small Methods*, 2018, **2**(4), 1700351.
54 C. Song, *et al.*, High peroxidase-like activity realized by facile synthesis of FeS2 nanoparticles for sensitive colorimetric detection of H2O2 and glutathione, *Biosens. Bioelectron.*, 2020, **151**, 111983.
55 X. Zheng, *et al.*, Peroxidase mimicking of binary polyacrylonitrile-CuO nanoflowers and the application in colorimetric detection of H2O2 and ascorbic acid, *ACS Sustain. Chem. Eng.*, 2021, **9**(20), 7030–7043.
56 X. Zhu, *et al.*, Nitrogen-doped carbon nanoparticle modulated turn-on fluorescent probes for histidine detection and its imaging in living cells, *Nanoscale*, 2016, **8**(4), 2205–2211.
57 J. Wang, *et al.*, Synthesis of imidazole-functionalized silicon quantum dots as "off-on" fluorescence probe for highly selective and sensitive detection of l-histidine, *Sens. Actuators, B*, 2016, **237**, 740–748.
58 T. Nagae, *et al.*, Colorimetric detection of histidine in aqueous solution by Ni2+ complex of a thiazolylazo dye based on indicator displacement mechanism, *Tetrahedron Lett.*, 2018, **59**(45), 3988–3993.
59 R. S. Bhosale, *et al.*, A 8-hydroxypyrene-1, 3, 6-trisulfonic acid trisodium salt (HPTS) based colorimetric and green turn-on fluorescent sensor for the detection of arginine and lysine in aqueous solution, *Sens. Actuators, B*, 2017, **241**, 1270–1275.
60 M. Zhang, *et al.*, Copper nanoclusters as probes for turn-on fluorescence sensing of L-lysine, *Talanta*, 2018, **182**, 595–599.
61 C. Chaicham, *et al.*, Effective GQD/AuNPs nanosensors for selectively bifunctional detection of lysine and cysteine under different photophysical properties, *Sens. Actuators, B*, 2019, **282**, 936–944.
62 F. Copur, *et al.*, Nanopaper-based photoluminescent enantioselective sensing of L-Lysine by L-Cysteine modified carbon quantum dots, *Sens. Actuators, B*, 2019, **279**, 305–312.